

---

## Exploring the mechanics of fish escape attempts through mesh

Vincent Benoit <sup>1,\*</sup>, Robert Marianne <sup>1</sup>, Simon Julien <sup>1</sup>, Vacherot Jean-Philippe <sup>1</sup>, Faillettaz Robin <sup>1</sup>

<sup>1</sup> IFREMER-STH/LTBH, Station de Lorient, 8 Rue François Toullec, 56100 Lorient, France

\* Corresponding author : Benoit Vincent, email address : [benoit.vincent@ifremer.fr](mailto:benoit.vincent@ifremer.fr)

---

### Abstract :

Predictive selectivity modelling is used to study fishing gear selectivity. These models rely on fish morphology parameters and fall-through experiments. Here, we developed a model of the mechanical interaction between a fish and a netting mesh during an escape attempt. In this model, the fish is described with three parameters: the first parameter measures its mechanical ability to penetrate a mesh and the others are body stiffness coefficients accounting for fish body deformation under mesh twine pressure. These parameters were identified from the results of a bench test simulating a fall-through experiment through a single 60-mm Polyethylene (PE) mesh. A rigid circular cone, a rigid elliptical cone and a small number of horse mackerel and haddock, offering a limited length range, were tested. Results were generalised and compared with those obtained on a piece of netting. Within the model's assumptions, it is possible to predict the success of an escape attempt if one knows the three fish parameters and the mesh load in normal and transverse directions. The study showed that escape potential is greater through an actual deformable mesh than through a non-deformable mesh. The potential size of this difference depends on the mesh load and orientation.

**Keywords** : Fish, Mesh, Escapement, Behaviour, Propulsion, Selectivity, Stiffness, Netting

# 1 Introduction

In Europe, the Common Fisheries Policy (Regulation (EU), 2013) focuses on minimizing the effects of fishing on a functioning ecosystem while maintaining the incomes of coastal communities. Since the beginning of 2019, this regulation, through total allowable catch (TAC) regulations (or Minimum Conservation Reference Size–MCRS–in the Mediterranean), prohibits the practice of throwing unwanted catch back into the sea. As a result, most European fleets need to reduce their discards to maintain their fishing opportunities. Changes in fishing gear selectivity and spatiotemporal fishing strategies are the two main strategies that fishermen can use to achieve this goal.

Fishing gear selectivity has been extensively studied, sometimes taking into account the behavioural response of fish to stimuli (Gatti et al., 2020; O’Neill and Summerbell, 2019; Glass and Wardle, 1995) or by observing behaviours without added stimuli (Robert et al., 2020). A trait-based approach has also been used to understand the operation of a selective device (e.g. Mouchet et al., 2019). However, most studies have focussed on the overall escape or retention of a selective device through a sorting process based on shape and fish size considerations. To take a mechanistic approach to selectivity considering the net characteristics and deformability depending on net load, the mechanism and success of an escape attempt thus need to be evaluated.

Fish capture mechanism has been studied for gillnets (e.g. Marais, 1985), where the mesh is made of monofilament or thin twine and is gently tightened by small floats on the upper rope. This characteristic makes bar tension rather low and the mesh largely deformable as a fish penetrates it. Consequently, for these fishing gears and assuming the fish attempts to pass through the mesh, the simple ratio of the mesh perimeter to the fish girth is one of the conditions for capture (Reis and Pawson, 1999) conditioned by the fish attempts to pass through the mesh. Towed fishing gears are subjected to hydrodynamic drag acting on the netting and the capture, which can result in much higher tensions in the mesh bars. Consequently, some authors (e.g. Efanov, 1987) have hypothesised that it is unlikely that a fish can distort the mesh when attempting to pass through it during most of the fishing process, except for large, strong fish. For small fish, Efanov’s assumption is based on a value of fish penetration force assumed to be 1.7 to 2.3 times its weight and a mesh bar tension of about 4 N in the case of a trawl bag moving at 2.3 to 3.1 knots. However, some evidence suggests that tension in the mesh bars can be low enough to enable distortion by a fish (O’Neill et al., 2003): square mesh usually has two bars with low tension; the capture built up in the codend leads to a progressive increase in mesh tension with potentially low values; the periodic motion of the vessel due to swell can also lead to a pumping effect in the codend with large variations in mesh tension.

The geometrical relation between the fish and the mesh to assess the success of fish escape through trawl codend meshes has been explored with the FISHSELECT method (Cuende et al., 2020; Herrmann et al., 2009). It is based on fall-through experiments, which provide binary results: a fish either falls or does not fall through a mesh. Practically, an operator presents each fish with a series of stiff mesh templates of different size and opening angles, cut from rigid plastic plate. Then, there is a modelling step simulating the experiments, which combines the fall-through results and the fish morphological data (cross-sections), allowing body deformation under the template pressure, to obtain the best penetration model for the fish. The upper and the lower parts of the fish body have different compression rates. The penetration force is assumed to be the fish weight (Cuende et al., 2020).

This paper takes a different approach by using virtual fall-through experiment based on the static mechanical balance of fish and mesh during an escape attempt in order to assess their interaction in detail. The main new hypothesis here is to suppose that the mesh—and not only the fish as in previous studies—can distort under fish action, which could result in escape success different from that found in a standard fall-through experiment. The force ranges (fish propulsion and bar tension) considered in the present study include Efanov's assumption (1987) in order to evaluate its hypothesis of non-deformation of the mesh. Although only one mesh characteristic is assessed, the mechanical model applies to any kind of mesh or netting. The collision of the fish body and the mesh twines is first modelled and solved, considering the friction and deformation of the fish body in this interaction, and used to identify a set of three parameters characterising the fish body by optimisation from experimental data. The modelled and experimentally reproduced escape successes are first compared for a small number of fishes for a given mesh with different openings in T0 and T90 configurations, then compared for escape successes through deformable and non-deformable mesh. The method is finally applied to netting to move towards its application to fishing gear.

## 2 Material and methods

The modelling of the fish body is presented in section 3.1. The fish escape mechanics are presented in section 3.2. Parameters involved in this modelling are identified using the data provided by a bench test and its experimental protocol, presented in section 3.3. The modelling of the mesh and the effects of its discretisation are presented in section 3.4. The way fish parameters are identified is presented in section 3.5. Details on how these parameters are applied to a 12 x 12 mesh netting are available in Section 3.6. The different case studies are described in Section 3.7.

### 2.1 Fish morphology and its deformability

A fish section shape is needed to solve the collision with the mesh. A continuous and smooth section definition is used to calculate the normal collision force vectors applied at the mesh point. In order to simplify experimental fish data collection, a simple elliptical shape was selected. The ellipse was defined by its minor and major diameters: respectively, fish width and fish height at the larger perimeter. In order to take the actual larger fish perimeter into account, the ellipse was scaled up or down so as to set its perimeter to the measured perimeter using the Ramanujan formulae (Villarino, 2006). Thus, the diameter ratio and the ellipticity remained unchanged. Perimeter was measured to the nearest millimetre with a supple measuring tape. The fish width and height were measured using a millimetre calliper. No fish compression was allowed during measurement.

In order to reduce the morphological measurement dispersion, several fish from the same species were grouped into perimeter classes, named CPe1, CPe2, etc. Perimeter was chosen as the most relevant parameter conditioning passage into a mesh (Purbayanto et al., 2003, Reis and Pawson, 1999, Kim, 2019). Moreover, the perimeter aggregates fish width and height.

In the model, the fish body and fish section model are assumed to be deformable. The linear elastic law, Eq. (1), is supposed to drive this deformation. Each section contour point in contact with a mesh

element is subjected to a collision force  $F_{\text{collision}}$  and is able to move toward the inside of the fish section in the normal direction, causing a depression  $d$ .

$$d = \frac{F_{\text{collision}}}{K_{\text{fish}}} \quad (1)$$

An investigation of fish deformation ability under simple finger pressure revealed that dorsal and ventral compressibility can differ (Tokaç et al., 2018). Thus, two stiffness coefficients  $K1_{\text{fish}}$  (ventral) and  $K2_{\text{fish}}$  (dorsal) are used here to model fish body deformation. These two elasticity laws are applied symmetrically on both sides of the minor axis. Considering the fish section symmetry (ellipse), the ventral and dorsal terms are not used in the results section.

## 2.2 Modelling escape mechanics: the collision between the mesh twines and the fish

Two mechanisms are considered in the escape mechanics modelling: (a) the friction force of the fish skin on the mesh twines due to fish propulsion and (b) the deformation of the fish body under the twine pressure. The friction supposedly involves two parameters: a friction coefficient  $\mu$ , forming a linear relation between the normal and the tangential forces (Coulomb, 1821) and the geometry of the fish body near the twine (Fig. 1).

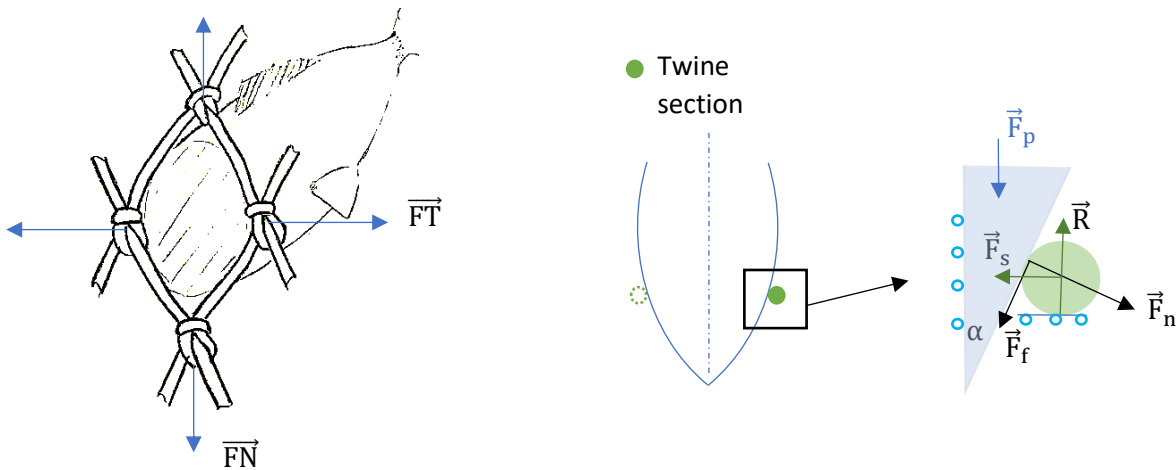


Fig. 1. Left: a fish passing through a mesh. The mesh is subjected to a normal force (FN) and a transverse force (FT). Centre: view from above of the symmetric bidimensional sketch of the fish passing through the mesh, represented by the green dots. Right: a zoom of the local fish/twine interaction. The blue circle accounts for slide links: the only possible motion is in the circle alignment direction. The elementary fish propulsion force  $\vec{F}_p$  is decomposed into a friction force  $\vec{F}_f$  tangent to the fish body, a force normal to the fish body  $\vec{F}_n$ , a force opposed to the mesh stretch  $\vec{F}_s$  due to the netting. The twine section vertical motion is supposed to be blocked by the horizontal slide links which apply the reaction force  $\vec{R}$  on the twine.

If we consider a fish passing through a mesh (Fig. 1, left), the mesh is subjected to a normal force FN (the normal direction refers to the direction normally used in traditional trawl assembly) and a transversal force FT. We assume the mechanical problem is symmetrical (Fig. 1, centre) with a vertical symmetry plane. This means that fish motion during mesh penetration is normal to the mesh plane. We consider the static equilibrium of the twine section (green disc Fig. 1, right) under the fish action modelled by a wedge (blue).

The static equilibrium of the twine can be written:  $\vec{F}_f + \vec{F}_s + \vec{F}_n + \vec{R} = 0$ . Where  $\vec{R} = -\vec{F}_p$ .

Forces are projected on the horizontal and vertical axes leading, respectively, to the relations:

$$\begin{cases} F_f \cdot \sin \alpha - F_n \cdot \cos \alpha + F_s = 0 \\ F_p = F_f \cdot \cos \alpha + F_n \cdot \sin \alpha \end{cases}$$

where  $\alpha$  is the angle between the symmetry axis and the fish body in contact with the twine.

Coulomb's law states that the force moduli of  $\vec{F}_n$  and  $\vec{F}_f$  follow the relation  $F_f = \mu F_n$ , where  $\mu$  is a dimensionless friction coefficient between the twine and the fish body. Assuming  $\mu \cdot \sin \alpha \approx 0$ , the relation between the mesh stretch force  $F_s$  and the propulsion force  $F_p$  is given by:

$$\frac{F_s}{F_p} = \frac{\cos \alpha}{\sin \alpha + \mu \cdot \cos \alpha} = A(\alpha, \mu) \quad (2)$$

The collision of the fish and the mesh twines is modelled by a series of fictitious springs acting normally to the fish surface at the contact points with the twines. A similar approach was taken by Le Bris and Marichal, (1999) for modelling to prevent collision of netting panels in fish farms. The spring stiffness  $K_{\text{collision}}$  was chosen so as to minimize the unrealistic penetration of the twines in the fish body model and to enable calculation convergence, as the condition number of the matrix equation increases with this stiffness.

In a spring mass approach, each mesh twine is split into several rigid bars to model its bending stiffness (Vincent et al., 2020). Spring forces are located at the resulting nodes connecting two adjacent bars.

In order to simplify the algorithms, the fish body remains undeformed during calculation, but a fictitious deformed body is considered in order to model its actual compressibility. There is a collision when the distance from a calculation mesh node to the deformed fish boundary model is lower than the twine radius  $r$  (Fig. 2). To prevent this unrealistic penetration, a force modelled with the spring equation (Eq. (3)) acting on the twine was added.

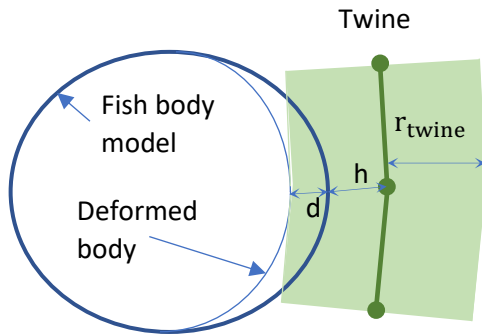


Fig. 2. Undeformed fish body model (thick blue line) and deformed body under twine pressure (thin blue line). Twine model, calculation nodes (dark green line) and limits of the actual twine (green).  $r_{\text{twine}}$  is the twine radius,  $h$  is the distance from the undeformed fish boundary to the nearest twine node,  $d$  is the fish deformation under twine action.

$$\begin{cases} h + d < r_{\text{twine}} \\ F_{\text{fish} \rightarrow \text{twine}} = -F_s = F_{\text{collision}} = K_{\text{collision}}(r_{\text{twine}} - h - d) \end{cases} \quad (3)$$

where  $r_{\text{twine}}$  is the twine radius and the threshold distance from calculation nodes for collision detection.  $K_{\text{collision}}$  is the stiffness of the springs modelling the collision forces at each twine node in contact with the fish.  $h$  is the distance from the undeformed fish boundary to the nearest twine node.  $d$  is the fish deformation under twine action, involving the fish body stiffness  $K_{\text{fish}}$  and the linear deformation model (1). Combining the fish body deformation  $d$  in Eq. (1) with Eq. (3) leads to:

$$\begin{cases} h + d < r_{\text{twine}} \\ F_{\text{collision}} = \frac{(r_{\text{twine}} - h)}{\frac{1}{K_{\text{fish}}} + \frac{1}{K_{\text{collision}}}} \end{cases} \quad (4)$$

Equation (4) is a standard spring model with a pseudo stiffness composed with  $K_{\text{collision}}$  and  $K_{\text{fish}}$ . When  $K_{\text{collision}}$  tends towards infinity, the pseudo stiffness tends towards  $K_{\text{fish}}$ . In the case where we assume the fish body to be non-deformable, the pseudo stiffness is simply  $K_{\text{collision}}$ . Successive tests to achieve spring deformation  $\ll$  mesh deformation made it possible to set its value at:

$$K_{\text{collision}} = 10^4 \cdot \text{AvgTwineTension}[N/m] \cdot \frac{1}{K_{\text{collision}}} \text{ is null.}$$

Each elementary fish force  $F_{\text{collision}}$  applied on an elementary portion of mesh twine is normal to the fish body at the contact point with the twine. It is integrated along the fish section in contact with the mesh twines to establish a relation between the penetration force and the opening force acting on the mesh twines. Considering that the friction coefficient  $\mu$  and the fish body angles are hardly measurable, particularly when the fish body is locally deformed by the twine pressure, the coefficient  $A(\alpha, \mu)$  (Eq. (2)) is assumed to be a constant for a given case study, i.e. regardless of the fish body length for a given species.

Thus, three parameters are considered to model the escape mechanics: a coefficient  $A$  linking the propulsion and the mesh spread force, and two coefficients  $K1_{\text{fish}}$  and  $K2_{\text{fish}}$  defining the ventral and dorsal elasticity.

$A(\alpha, \mu)$  is the ratio between the spreading force and the propulsion force. The fish can escape through the mesh if its propulsion force  $F_p$  is large enough to spread the mesh sufficiently. Thus, we use the term “**escape threshold**” defined as  $A(\alpha, \mu) \cdot F_p$  in the following paragraphs. From the discrete point of view, a fish can pass through a mesh, under initial load (FN, FT), if the inequality (5) is verified.

$$\sum_{\text{contact nodes}} F_{\text{collision at FN,FT}} < A(\alpha, \mu)F_p \quad (5)$$

Equation (4) and equation deriving from inequality (5) were introduced in the netting dynamics solver, detailed by Vincent et al. (2020) to solve the mechanical balance between the mesh and the fish and to establish a relation between fish propulsion force and the success of escape through a mesh.

Additional forces in the mesh plane (N,T) are added to the fish so as to void the resulting node forces on the fish section. The static fish balance is verified at each step of the simulation. This force allows the fish section to move in the plane (N,T) to the position corresponding to its easiest way to escape.

We used the pull of gravity as a proxy for the fish swimming propulsion during mesh penetration, following Krag et al. (2011). Supposing the propulsion force to be equal to fish weight is also a common assumption in fall-through experiments (Tokaç et al., 2018).

A hypothesis must still be made regarding the behaviour of the netting surrounding the escape mesh. When the fish is inside the mesh, FN and FT are modified because of the restoring forces of the surrounding meshes. In order to design a practically feasible bench test and to consider the surrounding meshes, we suppose these forces are such that the mesh cannot shrink but can stretch: the two opposite nodes cannot move inwards but can move outwards, the static equilibrium of nodes under the twine force being verified. In other words, the surrounding meshes will prevent the mesh from shrinking but cannot prevent the mesh from stretching, as supple twines do not support compression force. In the case of rigid twine material (e.g. coated or impregnated twine), this hypothesis could be invalid and the penetration simulation on a netting with adequate stiffness properties would be required.

An 'escape threshold' field can be established by simply sweeping FN and FT and calculating  $\sum_{\text{contact nodes}} F_{\text{collision}}$  at each point. However, this process can be time consuming, depending on sweeping finesse. Thus, a search algorithm was developed, based on an explicit Euler method, to search the 'iso escape threshold'. In both cases (sweep or search method), the basic simulation steps are:

- 1/ Solve the static mesh equilibrium under load ( $FN_i, FT_i$ ) with no fish.
- 2/ Insert the section of the fish in the mesh and solve the static mesh equilibrium with collision forces. N or T mesh displacements are blocked as discussed above.
- 3/ Calculate the escape threshold  $A(\alpha, f) \cdot F_p$ .
- 4/ Iterate until equation deriving from Eq. (5) is solved for the 'search method'.

The mesh is thus able to open when interacting with the fish and would, consequently, enable a larger fish to pass through compared to a non-deformable mesh. In order to compare the escape potential through deformable and non-deformable meshes (i.e. in a typical fall-through experiment with shapes cut from a rigid plastic sheet (Tokaç et al., 2018)), the mesh deformation was disabled in the simulator. Then, we compare the diameter ratio between the actual fish diameters (minor and major) and the largest fish diameter that could pass through the non-deformable mesh before it gets enlarged by the fish passage. This ratio is applicable to both the major and minor fish diameters. In other words, it shows the relative increase in diameter due to mesh deformation.

### 2.3 Experimental bench test and protocol

A bench test was designed and built to assess which load applied to a test mesh would allow the passage of a fish or a fish model through a single mesh (Fig. 3). It was designed as a fall-through experiment where the fish attempts to pass through the mesh under its weight force alone. As shown in Fig 3., the test mesh is set horizontally. Two force sensors measure FN and FT. Two linear actuators including position sensors enable the mesh shape and tension to be controlled. Mesh opening control and sensor readings are handled by a microcontroller program. The test protocol is detailed in Fig. 4.

A design choice was made so as to match the behaviour of an actual trawl netting: in T0 mode, we assume the T0 netting axial stiffness is such that the mesh opening in the N direction will not decrease when the fish open the mesh to pass through. Thus, the N direction actuator is blocked before the operator attempts to pass the fish. The same choice was made for T direction in the case of a T90 netting, which is probably a weaker hypothesis considering the lower stiffness (due to bending) of the T90 orientation.

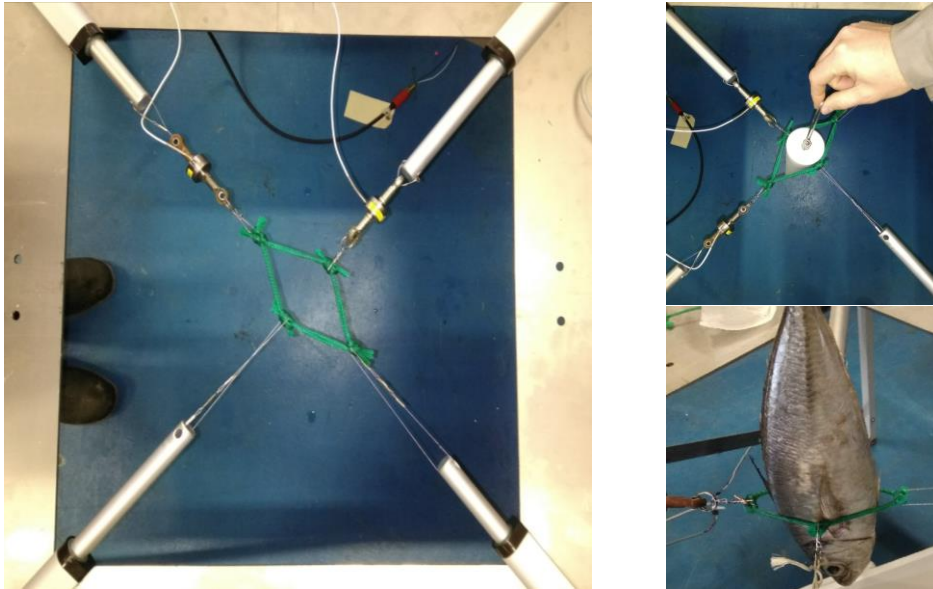


*Fig. 3. From left to right (1) overview of the experimental setup: the mesh, the four actuators and the two load cells. (2) Trying to pass a circular cone. (3) Trying to pass a horse mackerel.*



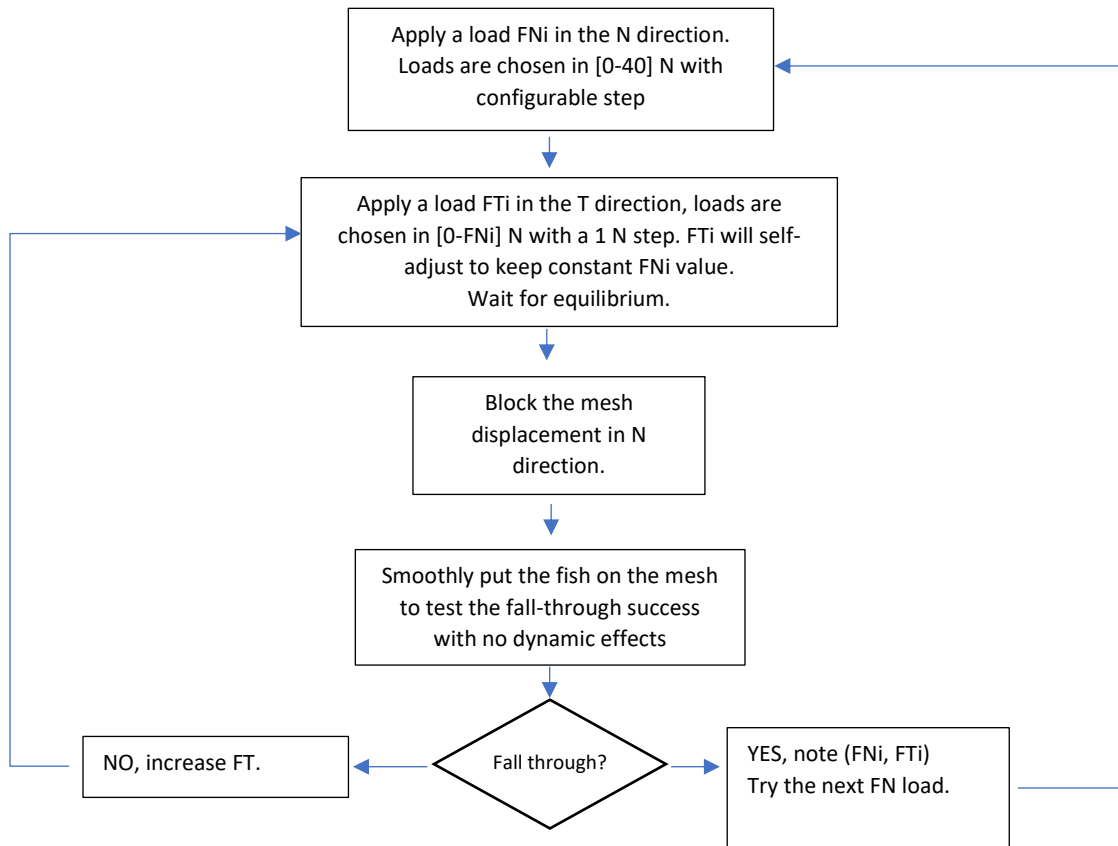


Fig. 4. Bench test protocol. The algorithm is explained here for T0 mode. In case of T90 mode, forces FT and FN and directions N and T are swapped. Moreover, the fish is presented so as to facilitate its passage: in T90 mode, the fish height is parallel to the T direction. In T0 mode, the fish height is parallel to the N direction.

The links between the mesh and the actuators could introduce elasticity in the N and T directions that would complicate interpretation of the results. These elasticities were identified using the bench test load cells and actuator position sensors and was roughly estimated at 12000 N/m in the N direction and 16000 N/m in the T direction. Although elongations induced by these stiffnesses are rather small compared with mesh elongation and fish deformation, these elasticities are taken into account in the mesh model.

The bench test also served to apply an aging cycle to a novel mesh before a test so as to respect the protocol described by Vincent et al. (2020).

The FN and FT ranges were chosen so as to be representative of actual tensions found in a codend or an extension piece of a 24-m trawler. Considering the results provided by Priour and De La Prada (2015), the observed mean variation in trawl drag due to catch load was around 400 daN from an empty codend to a full one. A codend with 100 meshes in its perimeter leads to a mean tension per twine of  $4000/200 = 20$  N. In order to consider a wider range of situations, we designed the bench test with a [2 N – 40 N] force range. This range includes the value of 4 N assumed by Efanov (1987).

Data obtained with this bench test are couples of forces ( $F_{Ni}$ ,  $F_{Ti}$ ) defining the limit where the fish can pass through the mesh. The points ( $F_{Ni}$ ,  $F_{Ti}$ ) are then represented in the plane ( $F_N$ ,  $F_T$ ). These points are then represented by linear regressions.

## 2.4 Modelling the mesh and discretisation effects

The mesh and the netting studied were modelled using the approach detailed by Vincent et al. (2020). According to this method, each mesh is split into several elastic bars (axial rigidity). The flexural rigidity  $EI$  is modelled by torques added at nodes between two adjacent bars. An angle at rest (i.e. without flexural torque) is imposed and the physical knots are modelled with additional bars of a given length  $L$  (Fig. 5), giving the mesh its actual hexagonal shape. These three mesh parameters were identified from experimental data in the previous study (Vincent et al., 2020). Mesh characteristics considered in the present study are detailed in Table 1.

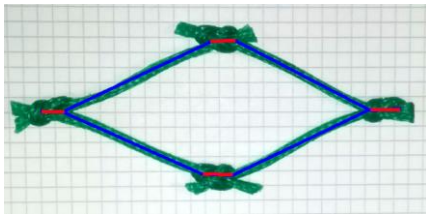


Fig. 5. The physical knots are modelled with additional bars (red segments). Considering the bar number (red and blue segments), this diamond mesh can be modelled as a hexagonal mesh.

Table 1. Physical properties of the mesh used in this study

Twine diameter x length between knots	Flexural rigidity $EI$ [N/m <sup>2</sup> ]	Rest angle [°]	Knot model length [mm]	Twine axial elasticity [N]
PE 4 mm x 60 mm	8.84e-05	40.21	8.86	5034

The mesh dynamics are solved using Newton's second law applied to nodes to reach a static equilibrium. Additional length conditions are solved to impose the linear twine axial elasticity of the bars.

The forces involved in the collision between the fish and the mesh bars depends on the number of bars used to model the mesh involved in the bench test (discretisation step, Fig. 6). This number is assessed to determine the best compromise between calculation effort and result accuracy.

Several couples of normal and transverse forces were applied on the mesh, and the spreading force due to the presence of a circular cone (diameter 60 mm) was calculated for the different discretisations (Table 2). The spreading force for each discretisation was compared to the spreading force for the reference discretisation made of 16 bars per mesh side.

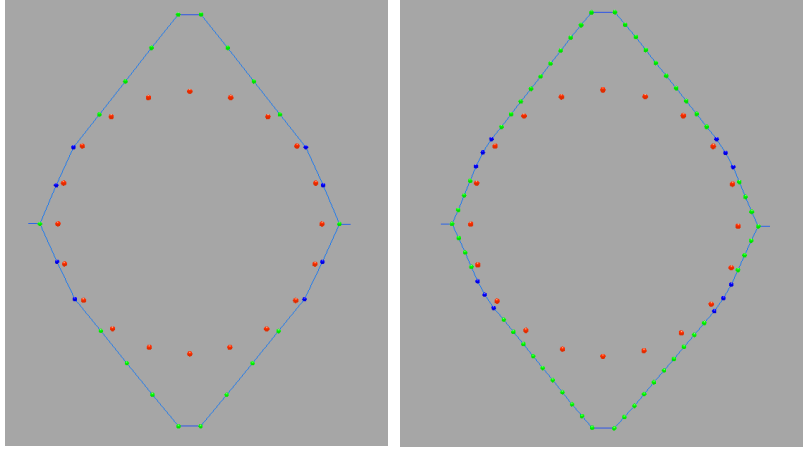


Fig. 6. The mesh side is modelled with 6 bars (left) and 16 bars (right). Green/blue spots denote the mesh calculation nodes. Red spots denote the limits of the circular cylinder, blue spots denote the contact points with the mesh twine. The twine radius is represented by the empty space between the red spot centres and the bars.

Table 2. Relative percentage difference of the mesh spreading force due to collision with the cone, 16 bar discretisation was taken as the reference value.

$\Delta$ % mesh spread force		Mesh side discretisation [bar number]					
		4	6	8	10	12	16
Mesh forces FN[N]	FT[N]						
1	200	-10.62	0.42	-0.14	<b>0.40</b>	-0.25	0.00
100	200	-36.79	1.11	-5.88	<b>0.38</b>	-1.17	0.00
200	1	-7.78	-2.27	-1.31	<b>-0.75</b>	-0.22	0.00
200	40	-13.17	-3.67	-1.40	<b>-1.34</b>	-1.07	0.00
40	200	-14.97	1.78	-0.55	<b>0.68</b>	-0.19	0.00
Mean relative percentage difference		16.67	1.85	1.86	<b>0.71</b>	0.58	0.00

One can observe a rapid convergence of the mean relative percentage difference to a nearly constant value for discretisation finer than 8 bars. Compared with the finest discretisation, the 10-bar discretisation leads to a maximum relative difference of 1.34% of the spreading force, which seems a reasonable compromise. Consequently, the discretisation level was set at 10 bars and all the results presented were obtained with this mesh side discretisation. This level is coherent with the level needed to model the twine flexural rigidity (Vincent et al., 2020).

## 2.5 Fish parameter identification

Three fish parameters  $A(\alpha, f)$ ,  $K1_{fish}$  and  $K2_{fish}$  were identified from the experimental results using an improved Nelder–Mead optimisation algorithm (Luersen et al., 1884). Experimental points resulting from fall-through experiments were modelled by linear regressions. The distances between the resulting lines and the simulated points were calculated at each optimisation step. The optimisation objective consisted in minimising the root mean square of the distances.

We hypothesised  $A$  is constant for a given species. In order to verify this assumption and the way  $K_{fish}$  depends on the fish perimeter, a single set of parameters was first calculated for each species using all its perimeter classes. We then calculated parameters separately for each perimeter class.

A preliminary and very rudimentary investigation of  $K_{fish}$  was done using a mm-graduated rule and a weight of 123 g (1.2 N). This force was applied to the fish skin using a shape similar to a mesh element of 6 mm length and 2 mm width corresponding to the discretisation of the mesh (60 mm, 10 bars). A width of 2 mm was chosen considering that the contact width of the twine is lower than its diameter. The depression  $d$  was measured at different points of two haddock and  $K_{fish}$  was calculated from Eq. (1). By doing so, we consider the fish stiffness involved in the interaction with a mesh element (a bar that discretises the mesh twine). Here, mesh discretisation is constant since otherwise, the stiffness would need to be normalised by the elementary bar length to avoid it being dependent on the mesh discretisation.

## 2.6 From a single mesh to netting

To design a realistic and feasible bench test and to ease the interpretation of the results, the modelling and experimental validations were performed on a single mesh. Then, we applied the model and its three identified coefficients to a 12 x 12 mesh netting (Fig. 7) to assess the escape threshold difference in a configuration closer to a full-scale fishing gear. This netting size was chosen to be large enough to let the over-tension due to fish penetration dissipate. We assumed a PE 4 mm x 60 mm 12 x 12 mesh netting to be sufficiently large to be representative of a bigger netting with regard to escape attempts for the considered material.

Two different behaviours of knots at the limits of the netting panel are considered: (1) the boundary nodes are free to move when the fish is penetrating and the FN and FT boundary forces remain constant, or (2) the boundary nodes are blocked and the FN and FT forces can evolve during fish penetration. Moreover, the surrounding mesh (mesh outside the 12 x 12 panel) would prevent the panel from shrinking but let the panel stretch (cf. end of section 2.2).

The netting size is large enough if the boundary conditions (i.e. positions or forces imposed at the netting boundaries) are not significantly affected by the fish escape attempt. If affected, the success of the attempt (escape threshold) must not be significantly modified. In the case of an actual escape, boundary conditions would be intermediate: knots would move and forces would change because of the surrounding knot action.

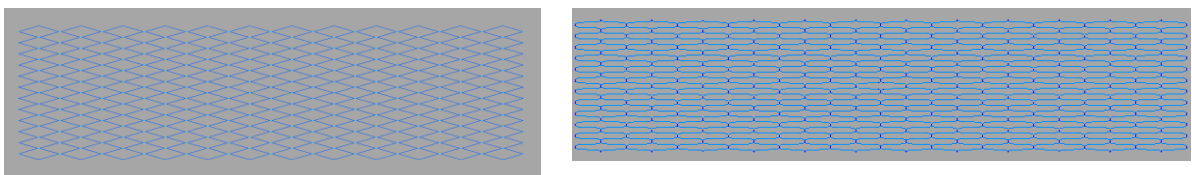


Fig. 7. The 12 x 12 mesh netting before an escape attempt. Left: T0 mode with FN = 51.2 N and FT = 14.8 N. Right: T90 mode with FN = 2.07N and FT = 97.8N. Forces are the sum of the boundary forces before penetration. Thus, mesh force will be divided by 12.

## 2.7 Case studies

We considered different case studies, including plastic models and actual fish. The former consisted of (1) a rigid circular cone made of machined POM (polyoxymethylene) plastic (Table 3), and (2) a rigid elliptical cone made of PLA plastic (Polylactic acid) built up by a 3D printer (Table 4). The theoretical value of A was calculated for these rigid cones from their angles and their supposed friction coefficients using Eq. (2).

The other case studies were (3) haddock (Table 6) and (4) horse mackerel (Table 7), whose characteristics are presented in Table 5 to Table 7. Considering the time needed to bench test a fish, their numbers were limited. The horse mackerels were divided into three perimeter classes and the haddock into two perimeter classes.

The elliptical cone and the fish were oriented so that their height was parallel to the N direction of the mesh in T0 mode and parallel to the T direction in T90 mode.

Table 3. Characteristics of case study 1: a rigid circular cone


	Length [mm]	200
	Large diameter [mm]	60
	Large perimeter [mm]	188.50
	Small diameter [mm]	20
	Half Angle [°]	5.71
	Weight Fp (in air) [N]	4.01
	Friction coefficient (POM on PE)	0.086 (Yamaguchi Y., 1994)
	Fish Stiffness 1 [N/m]	Infinity
	Fish Stiffness 2 [N/m]	Infinity
	Theoretical A value	5.38 (Eq. (2))
Theoretical A·Fp value [N]	21.57	

Table 4. Characteristics of case study 2 : a rigid elliptical cone. Lead weights were added to increase Fp.


	Length [mm]	90
	Large ellipse diameters [mm]	65 x 36
	Large perimeter [mm]	161.9
	Small diameter [mm]	54 x 27
	Half Angle [°]	2.86 to 3.50
	Weight Fp (in air) [N]	2.27
	Friction coefficient on PE	0.10 (Yamaguchi Y., 1994)
	Fish Stiffness 1 [N/m]	Infinity
	Fish Stiffness 2 [N/m]	Infinity
	Theoretical A value	6.56 based on 3° angle
Theoretical A·Fp value [N]	14.80	

Table 5. Main characteristics of studied fish.

	Number	Size range [mm]	Mass range [g]	Larger perimeter range [mm]	Larger height range [mm]	Larger width range [mm]
Haddock	7	305 – 335	265 – 347	140 – 166	52 – 67	34 – 38
Horse mackerel	13	335 – 375	332 – 545	172 – 205	65 – 76	41 – 54

Table 6. Case study 3: haddock. Characteristics and corrected height and width of the two perimeter classes, taking the actual larger perimeter into account.

Haddock perimeter class	Avg mass [g]	Avg perimeter [mm]	Avg height [mm]	Avg width [mm]	Avg length [mm]	Corrected height [mm]	Corrected width [mm]
CPe1	306	148	56.7	35.3	318	57.4	35.8
CPe2	317	162	64.5	35.8	322	65.0	36.0

Table 7. Case study 4: horse mackerel. Characteristics and corrected height and width of the three perimeter classes, taking the actual larger perimeter into account.

Horse mackerel perimeter class	Avg mass [g]	Avg perimeter [mm]	Avg height [mm]	Avg width [mm]	Avg length [mm]	Corrected height [mm]	Corrected width [mm]
CPe1	389	178	66.6	44.4	351	67.3	44.8
CPe2	462	190	70.3	48.0	365	71.2	48.6
CPe3	508	199	74.5	50.5	369	75.0	50.9

### 3 Results

#### 3.1 Incompressible cones (case studies 1 and 2)

Experimental threshold points in the fall-through bench test were modelled with linear regressions, as detailed in

Table 9. Each cone coefficient  $A$  was optimised to fit the experimental data. Optimisation results are presented in Table 10. The optimal values obtained were  $A \cdot F_p = 41.34$  N for the circular cone and  $A \cdot F_p = 13.61$  N for the elliptical cone. Experimental points and regression lines are shown in Fig. 8 (right panel).

Using the collision model, forces FN and FT were swept in order to build an escape thresholds field calculating the term  $\sum_{\text{contact nodes}} F_{\text{collision}}$  of equation (5). Fig. 8 (left panel) shows different iso level contours. The threshold value is written for some contours. Each contour has a part in a region where FN > FT, which corresponds to a mesh working in T0 mode (main force in N direction), and a part in a region where FT > FN, which corresponds to a mesh working in T90 mode (main force in T direction). If a mesh load (FN, FT) is inside the iso value  $A \cdot F_p$  contour (in the grey area containing the diagonal FN = FT), the collision model predicts that the cone can pass through the mesh, otherwise, if the point (FN, FT) is outside, it cannot pass. The values around FN = 0 and FT = 0 is undefined because of aberrant interpolation results. The circular cone iso level  $A \cdot F_p = 41.34$  N and the elliptical cone iso level  $A \cdot F_p = 13.61$  N are shown in Fig. 8 (left and right).

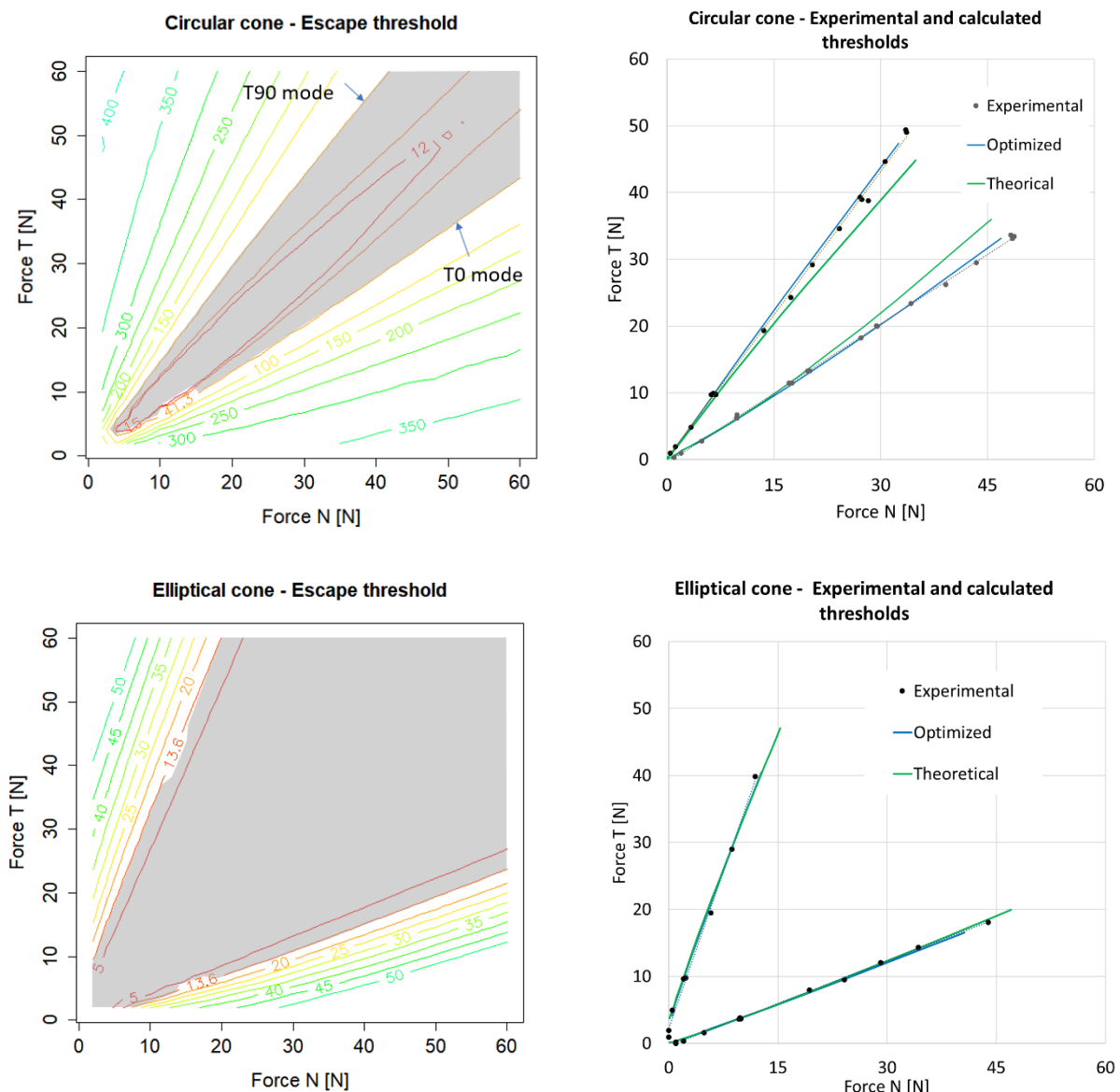


Fig. 8. Left panel: escape threshold contours for the rigid cones (case study 1 and 2) for different  $A \cdot F_p$  values. The optimal escape threshold  $A \cdot F_p = 41.34$  N (circular cone) and  $A \cdot F_p = 13.61$  N (elliptical cone) to fit experimental data is the limit of the pass-through zone for the considered weight (a pass is possible inside the grey area). Right panel: comparison of experimental data (black dots), escape threshold for optimised A (blue) and escape threshold for the theoretical A (green).

The diameter ratio between the present cone diameter and the largest diameter that could pass through the non-deformable mesh (before it gets enlarged by the cone's passage) is presented Fig. 9. In the T90 case with the elliptical cone, the ratio is not provided for T forces below circa 5 N because it does not correspond to a physical solution.

For instance, for the mesh load  $F_N = 40\text{ N}$ ,  $F_T = 20\text{ N}$  and the circular cone, Fig. 9 (top left panel) shows a ratio of about 1.3. This means the diameter of the circular cone passing through the deformable mesh is 1.3 times greater than the same cone passing through a non-deformable mesh. Fig. 9 (right panels) presents the same result for the optimal A values for circular and elliptical cones. Low force values make the ratio increase as the mesh is more easily distorted.

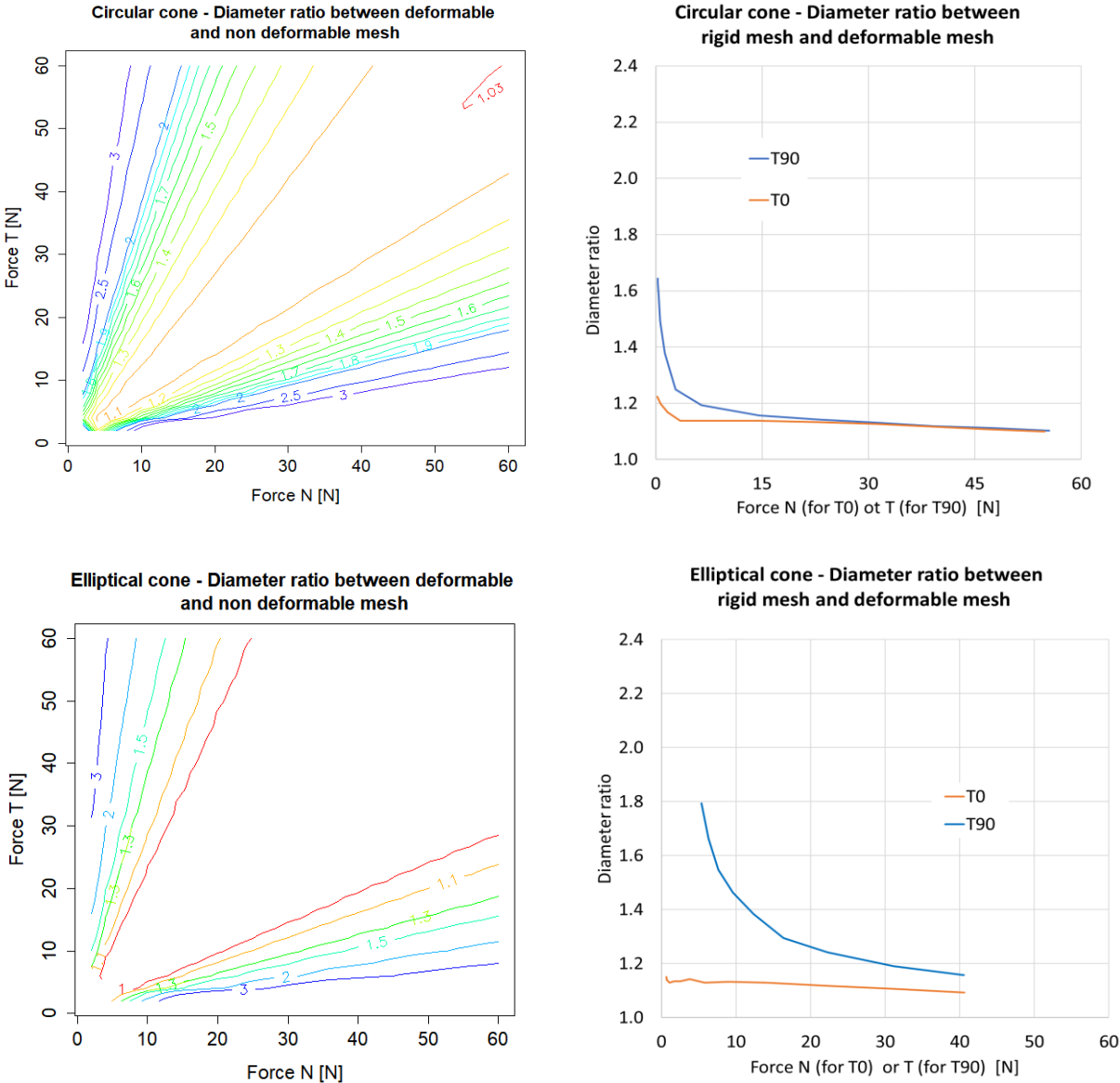


Fig. 9. Left: diameter ratios between rigid cones (case studies 1 and 2) passing through the deformable mesh and the same cones passing through the non-deformable mesh. Right: diameter ratios corresponding to escape threshold  $A \cdot F_p = 41.34\text{ N}$  for the circular cone and  $A \cdot F_p = 13.61\text{ N}$  for the elliptical cone in T0 and T90 modes.



### 3.2 Preliminary evaluation of $K_{fish}$

**Erreur ! Source du renvoi introuvable.** presents the measurement of the depression at a number of points on the bodies of two haddock. The average fish stiffness is deduced from Eq. (1).

Table 8. Measured values of  $d$  and calculated values of  $K_{fish}$



Fish length [mm]	280		320	
	$d$ [mm]	Avg $K_{fish}$ [N/m]	$d$ [mm]	Avg $K_{fish}$ [N/m]
Upper dorsal part	2	452	4	329
	3		4	
	3		3	
Side dorsal part	5	302	4	278
	3		4	
	4		5	
Ventral part	11	134	12	125
	7		9	
	9		8	

### 3.3 Haddock and horse mackerel (case studies 3 and 4)

Experimental threshold points resulting from the haddock and horse mackerel fall-through bench tests were modelled with linear regressions as detailed in Table 9 and the results are presented in Fig. 10. The three coefficients ( $A$ ,  $K_1$ ,  $K_2$ ) for each species were optimised once for all the perimeter classes. Optimisation results are presented in Table 10. The escape threshold values  $A \cdot F_p$  for the perimeter classes were respectively, 8.28 and 8.58 N for the haddock tested and 24.50, 29.10 and 32.00 N for the horse mackerel.

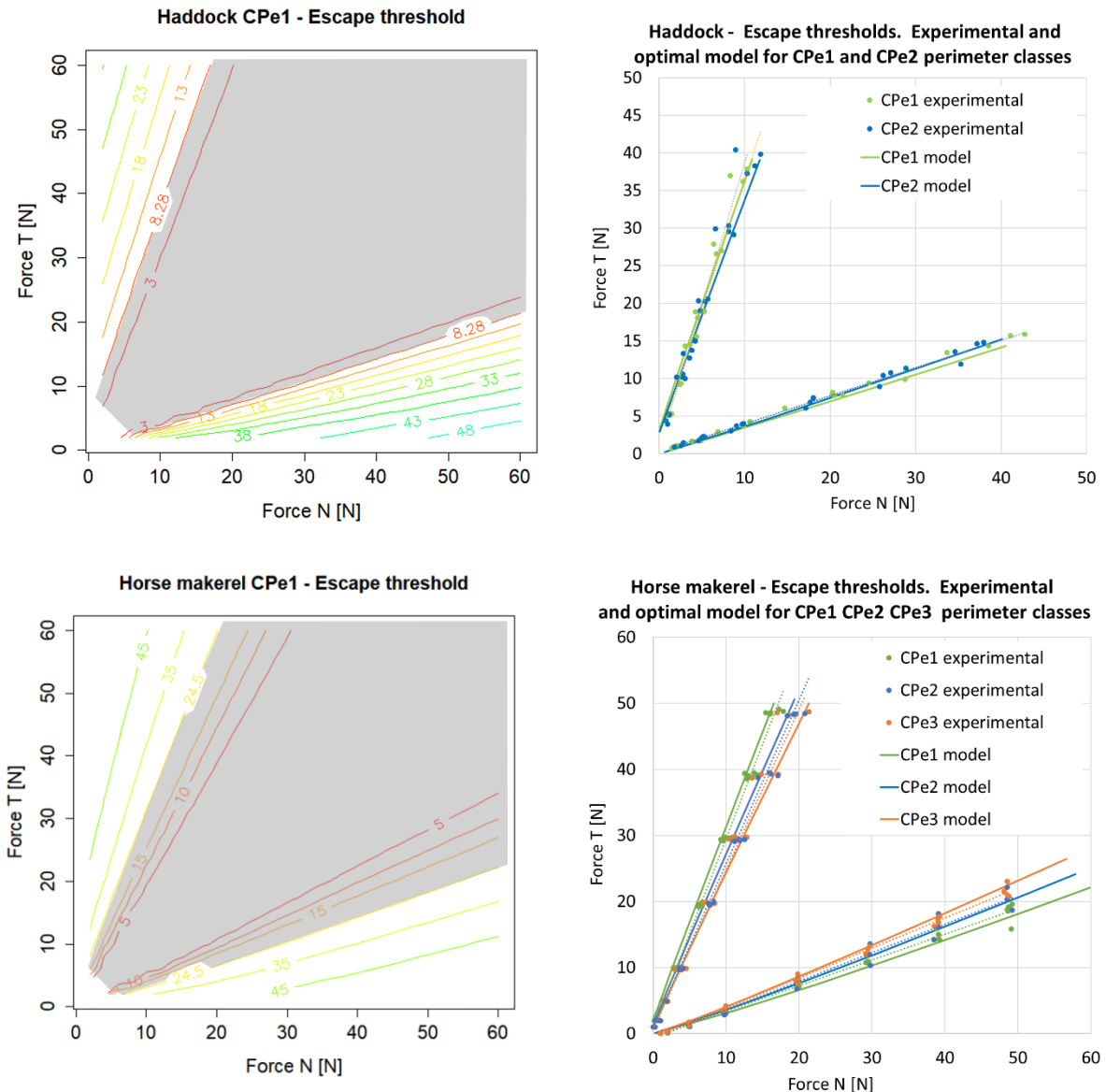


Fig. 10. Left panel: escapement threshold iso contours for the haddock and horse mackerel and pass-through zone for CPe1 (in grey). Note: the contour zigzags for the low loads are due to interpolation approximations but the figure on the right does not reproduce these zigzags. Right panel: experimental data and model with optimised A, K1 and K2 values.

The diameter ratios due to mesh deformation and maximum fish deformation are presented in Fig. 11. For instance (Fig. 11, left), a class 1 haddock passing through a deformable mesh set in T90 mode with a transverse load of 10 N can have diameters (minor and major) about 1.4 times larger than a fish passing through the rigid mesh with the same initial shape (before penetration), as illustrated in Fig. 12. This ratio increases when the mesh load decreases. A class 1 haddock passing through the mesh set in T0 mode with a normal load of 10 N, can have diameters (minor and major) about 1.1 times larger than a fish passing through the same rigid mesh. This ratio is only due to mesh deformation. The maximum fish deformation obtained from numerical simulation (Fig. 11, right) denotes the maximum depression of the fish body at one contact node of the mesh. This deformation is not symmetrical due to the different values of K1 and K2.

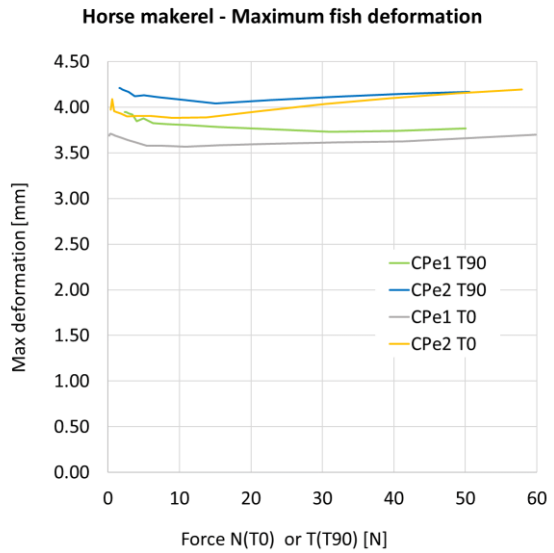
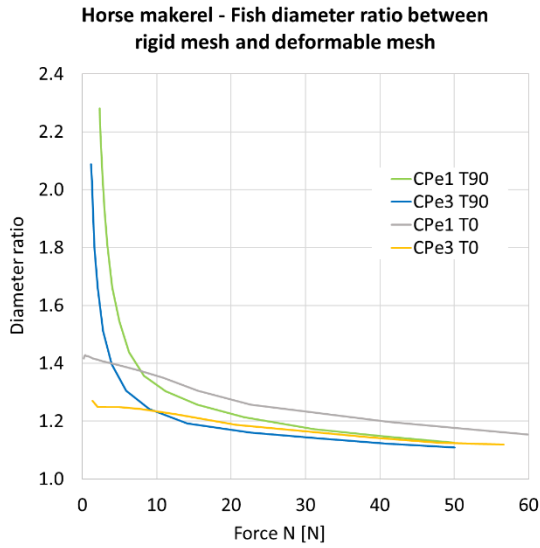
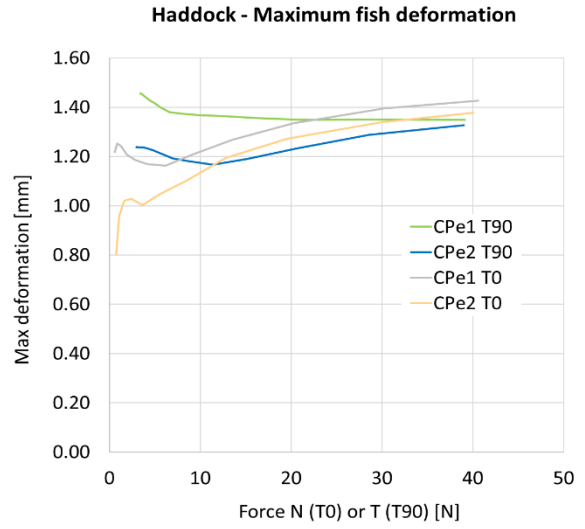
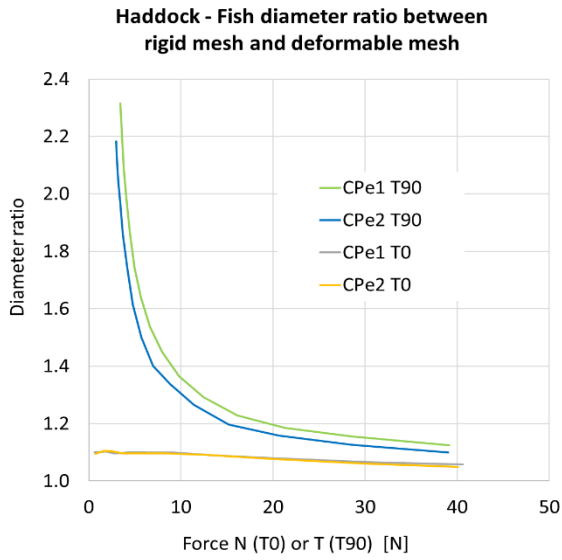


Fig. 11. Left panel: ratio between minor (major) diameters of a deformable haddock (horse mackerel) passing through a non-deformable mesh and a deformable mesh. Right panel: fish body maximum deformation when passing through the mesh. Simulation results.

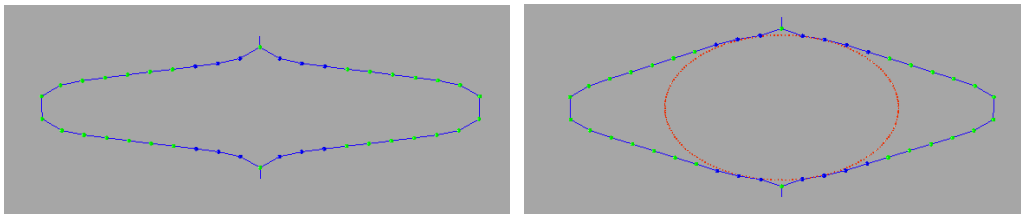


Fig. 12. Calculated mesh shape before and during fish penetration by a haddock. The T force is 6.6 N, the diameter ratio between a fish passing through the non-deformable mesh and the deformable mesh is about 1.5. The reason why the fish section seems to be in contact with the twine centre line is due to fish deformation, which is calculated but not represented.

Table 9. Linear models of experimental fall-through thresholds for the different case studies.

Case study		Linear regression equation	$R^2$
Circular cone	T0	FT = 0.6938 FN – 0.4313	0.9996
	T90	FT = 1.4479 FN + 0.0411	0.9992
Elliptical cone	T0	FT = 0.4239 FN - 0.3988	0.9993
	T90	FT = 3.1208 FN + 2.2813	0.9960
Haddock perimeter class CPe1	T0	FT = 0.3741FN + 0.2346	0.9889
	T90	FT = 3.8036FN + 0.7482	0.9720
Haddock perimeter class CPe2	T0	FT = 0.3700FN + 0.2472	0.9951
	T90	FT = 3.4836FN + 1.6456	0.9582
Horse mackerel perimeter class CPe1	T0	FT = 0.3900 FN - 0.5632	0.9926
	T90	FT = 2.8612 FN + 0.9076	0.9946
Horse mackerel perimeter class CPe2	T0	FT = 0.4310 FN - 0.7228	0.9834
	T90	FT = 2.4812 FN + 0.9050	0.9807
Horse mackerel perimeter class CPe3	T0	FT = 0.4547 FN - 0.6747	0.9964
	T90	FT = 2.4241 FN + 0.6111	0.9951

Table 10. Optimised coefficients A, K1 and K2 (when applicable) and RMS error. For case studies 3 and 4, optimised coefficients are presented for all classes of each species and separately for each class. Relative difference (in %) between the coefficient of each perimeter and the species coefficient is indicated in brackets.

	A( $\alpha, \mu$ )	K1 <sub>fish</sub> [N/m]	K2 <sub>fish</sub> [N/m]	RMS error [N]
Cylindrical cone	10.31	-	-	0.59
Elliptical cone	6.03	-	-	0.45
<b>Haddock perimeter classes CPe1, CPe2</b>	<b>2.76</b>	<b>525</b>	<b>635</b>	<b>2.81</b>
Haddock perimeter class CPe1	2.43 (-12%)	527 (+0.4%)	660 (+3.9%)	1.33
Haddock perimeter class CPe2	2.81 (+1.8%)	543 (+3.4%)	560 (-12%)	0.64
<b>Horse mackerel perimeter classes CPe1, CPe2, CPe3</b>	<b>6.43</b>	<b>322</b>	<b>474</b>	<b>4.50</b>
Horse mackerel perimeter class CPe1	5.58 (-13%)	358 (+11%)	351 (-26%)	0.24
Horse mackerel perimeter class CPe2	6.42 (-0.2%)	474 (+47%)	377 (-20%)	0.41
Horse mackerel perimeter class CPe3	6.95 (+8.1%)	437 (+36%)	367 (-23%)	0.25

The sets of parameters obtained by optimising all perimeter classes altogether or for each class separately do not lead to the exact same values. Escape thresholds are presented qualitatively on Fig. 13. The biggest differences appear for CPe2 haddock in T90 mode: if FT = 35N, FN changes of about 5%. Both strategies qualitatively provide the same escape values for CPe2 fish in T0 and T90 mode. For horse mackerel, the biggest difference appears with CPe1 fish in T0 mode: if FN = 40N, FT changes of about 6%.

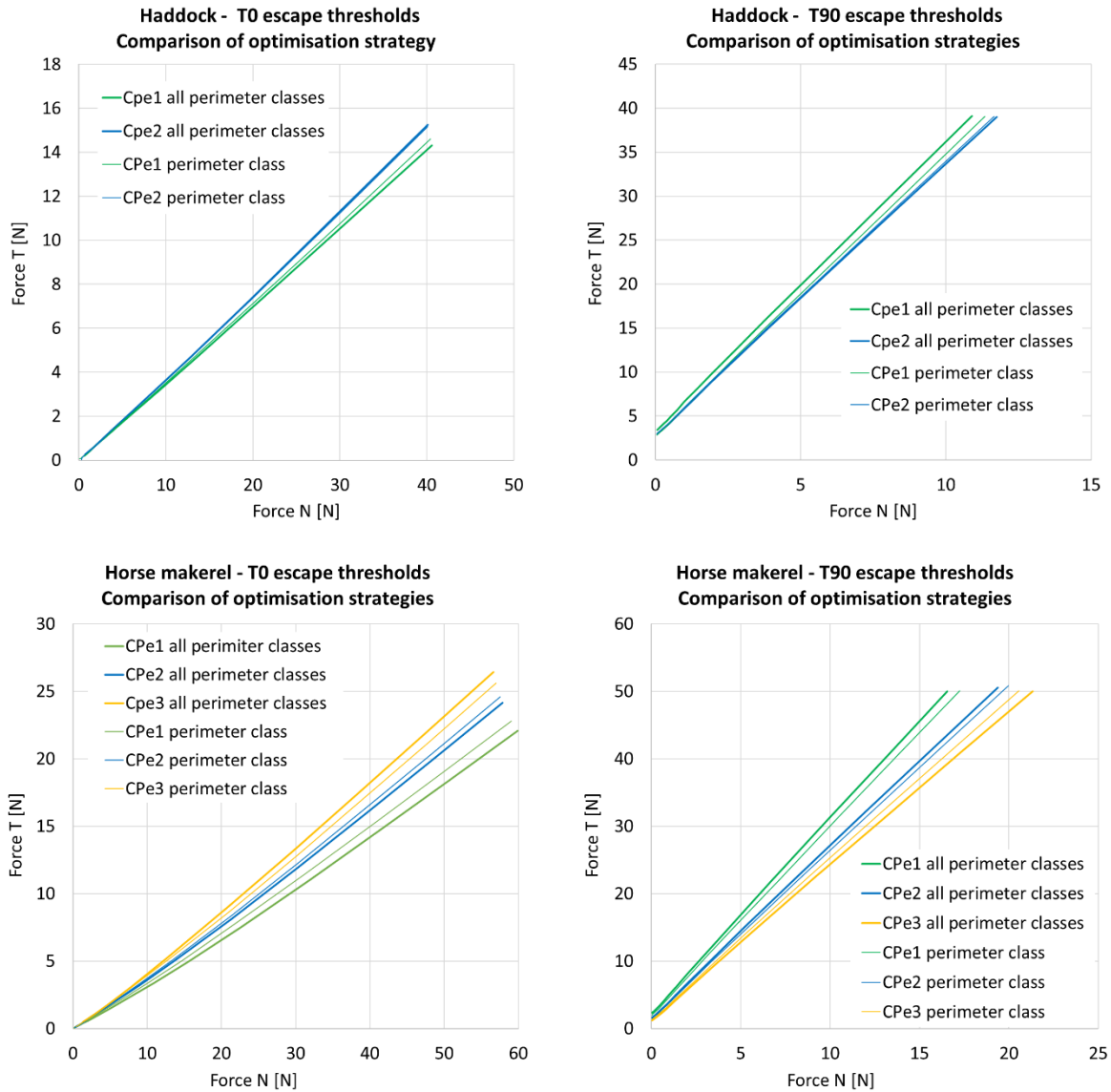


Fig. 13. Comparison of escape thresholds for haddock and horse makerel with parameters optimised for all perimeter classes and for each perimeter class. T0 (left) and T90 (right) were dissociated to make to reading easier.

### 3.4 From a single mesh to netting

Simulation views of the collision model applied to a 12 x 12 mesh netting made of the same material as the single mesh are shown in Fig. 14.

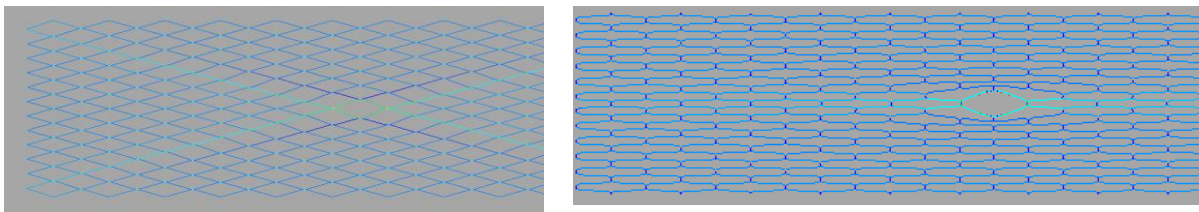


Fig. 14. The 12 x 12 mesh netting during a successful escape. Left: T0 mode with  $N = 51.2 \text{ N}$ ,  $T = 14.8 \text{ N}$ . Right: T90 mode with  $N = 2.07 \text{ N}$ ,  $T = 97.8 \text{ N}$ . Forces are the sum of the boundary forces before penetration. Thus, mesh force is to be divided by 12.

The escape thresholds through the central mesh of this netting were calculated for the rigid cones, haddock and horse mackerel (Fig. 15). We can observe that the thresholds for the single mesh and the netting are relatively similar for T0 mode. The thresholds for T90 mode allow an easier escape through the netting than through a single mesh, particularly for the circular cone and the horse mackerel.

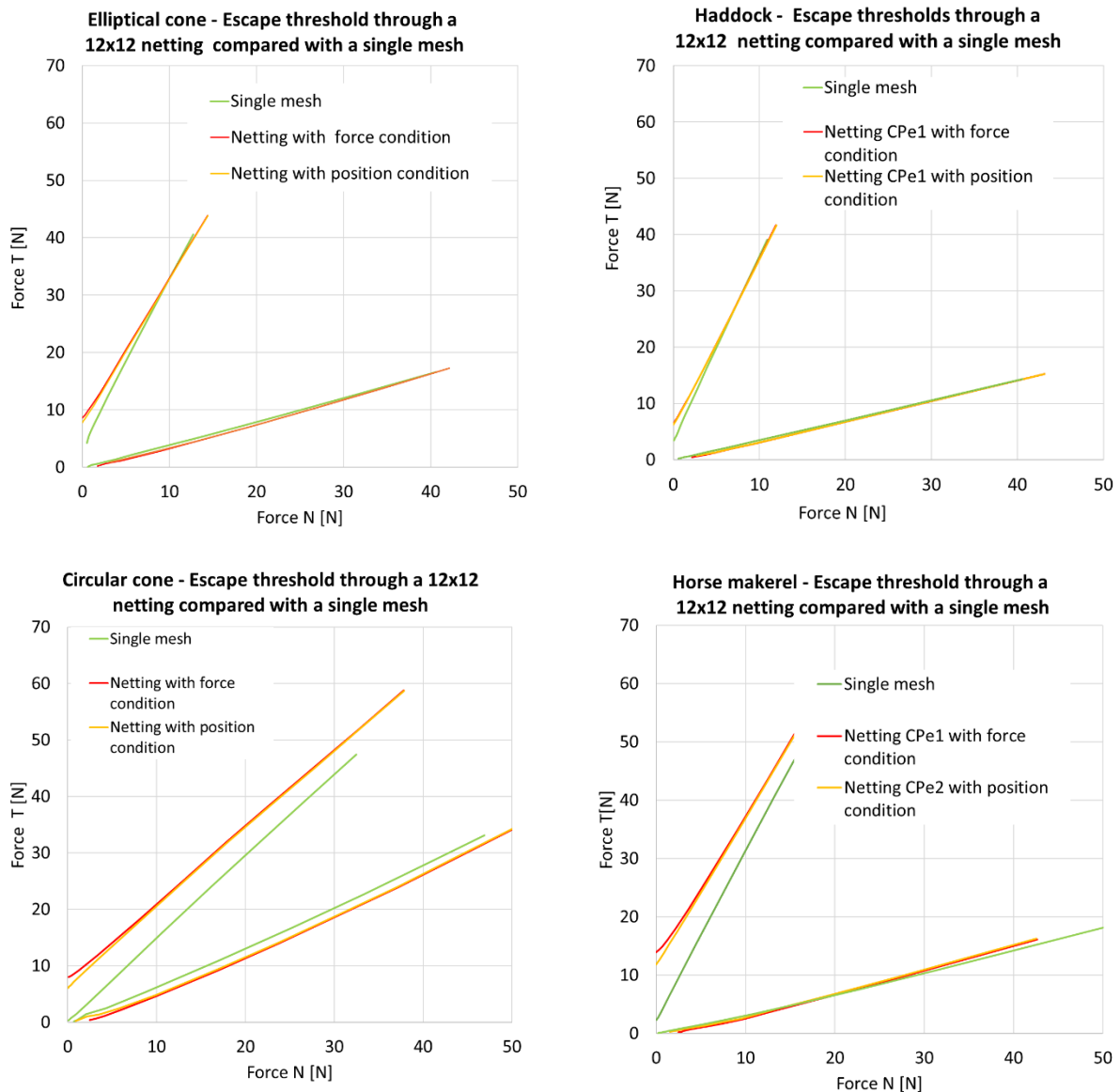


Fig. 15. Escape thresholds for the 12 x 12 mesh netting compared with the single mesh threshold. For each case, the effects of the boundary conditions are presented (force condition or position condition).

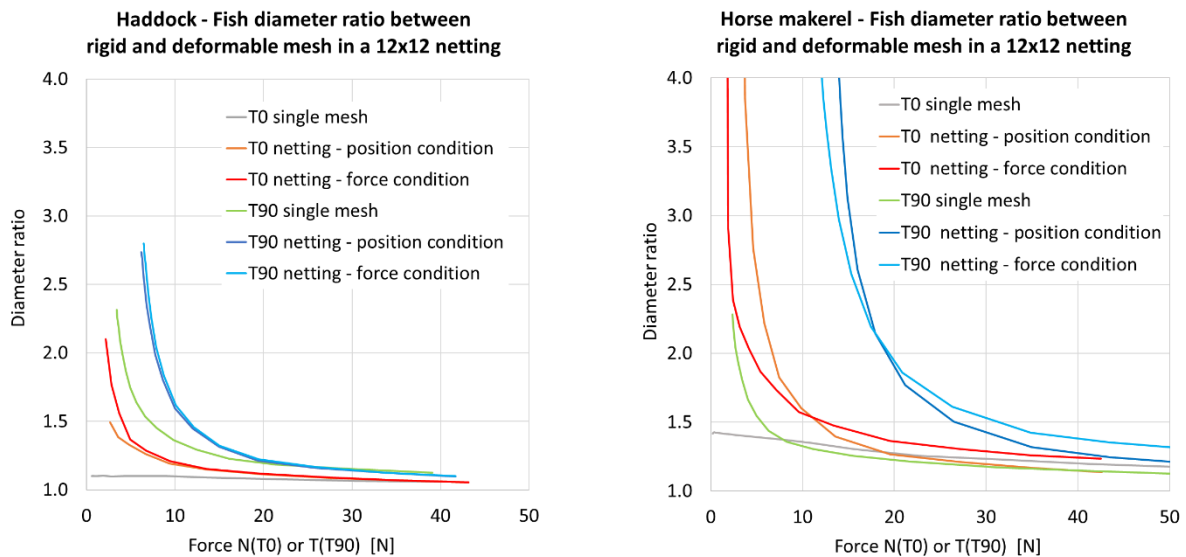
In order to explain these relative differences between case studies, a comparison of the relative geometry of the cones, fish and mesh is presented in Table 11. This table shows that the haddock and the elliptical cone are relatively similar in terms of diameter ratio (high values, from 1.61 to 1.81)

and in terms of perimeter ratio (low values, from 0.62 to 0.67). The circular cone and the horse mackerel are relatively similar in terms of diameter ratio (low values, from 1.00 to 1.50) and perimeter ratio (high values, from 0.74 to 0.83). The slopes of the experimental point linear regressions (Table 9) clearly differ only for the circular cone.

Table 11. Comparison of diameter and perimeter ratios for the different case studies. The mesh perimeter is 240 mm. Escape threshold slopes were obtained from 12 x 12 netting simulations.

	Diameter ratio (major/minor)	Perimeter ratio (fish/mesh)	T0 threshold slope	T90 threshold slope
Circular cone	1.00	0.79	0.70	1.39
Elliptical cone	1.81	0.67	0.42	2.50
Haddock (2 classes)	1.61 - 1.80	0.62 - 0.67	0.35	2.93
Horse mackerel (3 classes)	1.50 - 1.46 - 1.48	0.74 - 0.79 - 0.83	0.39	2.54

For the single mesh, Fig. 15 shows that the haddock and the elliptical cone are similar in terms of threshold at  $FN \approx 0$  (FT around 3 N). The circular cone and the horse mackerel thresholds are close to 0 when  $FT \approx 0$ . When considering the netting, the shift in FT is around 3 to 5 N for the elliptical cone and haddock and around 8 to 10 N for the circular cone and horse mackerel compared with the single mesh. The thresholds in T0 mode are relatively similar for the single mesh and for the 12 x 12 netting. The transition from a single mesh to the 12 x 12 netting increases the potential escapes in T90.



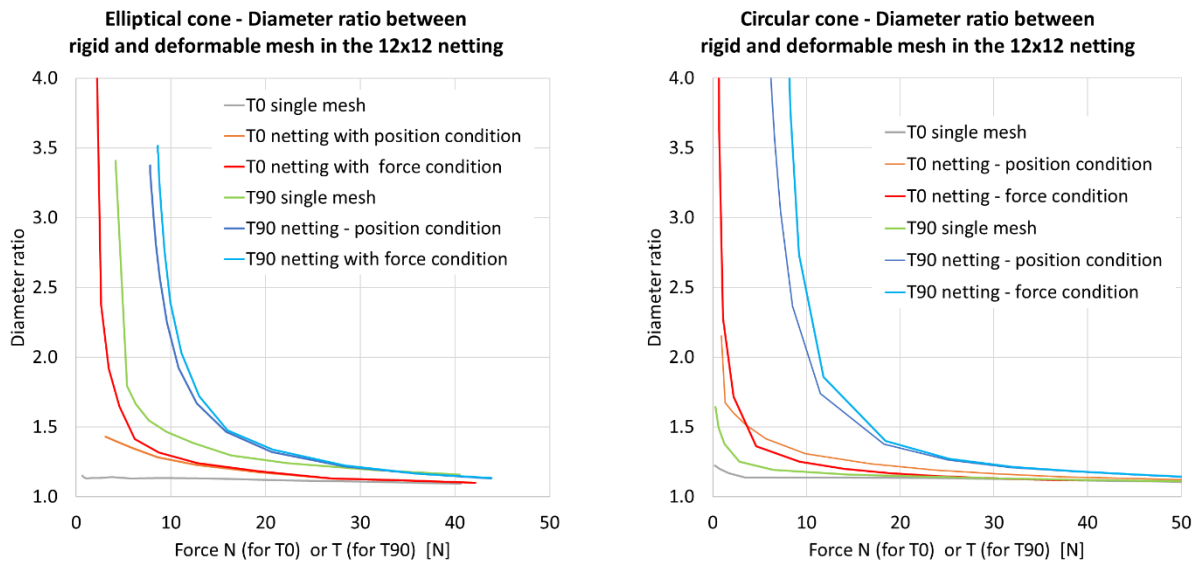


Fig. 16. Diameter ratios compared between a single mesh and the 12x12 netting for the different case studies.

Exploring the diameter increase between a rigid mesh and a deformable netting shows that the gain in T90 mode is greater than the gain in T0 mode but the diameter gain is greater for the netting than for the single mesh in both cases (Fig. 16). Some curves seem to tend toward infinity since the diameter passing through the rigid mesh tends toward smaller values when FN tends towards lower values. Fig. 16 also shows that the diameter ratios calculated with the boundary condition of force or position differ.

## 4 Discussion

### Hypothesis and general results

A model was developed to simulate the escape of a fish through a mesh, considering the fish motion to be normal to the mesh plane and that no dynamic effect could increase the penetration force. Since this study was a first attempt to deal with the deformation of the mesh, hydrodynamic effects were not considered. Yet, depending on the current orientation relatively to the fish body in a towed fishing gear, the hydrodynamic force would likely modify the escape success of fish. Some authors (Jones et al., 2008) observed a tendency towards higher mean escape rates at higher trawl speeds but the explanation is mainly behavioural. To our knowledge, there is yet any study describing the relation between the hydrodynamic forces acting on the fish body and the escape success. Still, a current oriented toward the outside of the net is unlikely to have the same effect on the escape success compared to a current parallel to the net pushing the fish toward a mesh twine and increasing the friction force; this question will be addressed in further research.

Here, results offer a new perspective on the topic by using an escape threshold in the mesh load plane (FN,FT) that is used to uniformize presentation for T0 and T90 modes: the fish escape is successful if the mesh load (FN,FT) is inside the escape threshold iso value, while loads outside of this curve prevent any escape.

For elliptical-shaped sections (Fig. 10 and to a lesser extent, Fig. 8), the escape threshold is non symmetrical (around the axis FN = FT) and confirms a known property of T90 netting used as a means of selectivity: the escape is easier for roundfish when the netting is turned 90° (Digre et al., 2010).



For instance, a mesh load of FN = 30 N, FT = 10 N (Fig. 10, Haddock) does not allow escape in T0 mode while a load FN = 10 N, FT = 30 N does allow escape in T90 mode.

The model involves three coefficients. When applied to the two rigid bodies (circular and elliptic cones), the model shows that A does not depend on the mesh load (FN, FT) in the considered range. For the two rigid bodies, the optimised values of A are greater than the theoretical values (94% and 7%, respectively). The error  $\Delta\mu$  of the cone friction coefficient leads to an error in A (Eq. (2)) close to 1 (using the general propagation of error formula:  $\Delta A = \Delta\mu \left| \frac{\partial}{\partial\mu} \left( \frac{F_p \cdot \cos\alpha}{\sin\alpha + \mu \cdot \cos\alpha} \right) \right|$  with  $\mu = 0.1$  and  $\Delta\mu = 0.03$ ). This cannot explain the difference between theoretical and optimized A values. The twine compression under the pressure of the cone and under the mesh tension could explain a part of this difference, as it lets it penetrate more easily. The twine compression is particularly significant for the circular cone as the surface contact with the twine is lower than for elliptic shapes (and the pressure on the twine higher). An important factor is the angle  $\alpha$ . The theoretical value of A with  $\alpha = 0$  is 10 for the circular cone ( $\mu = 0.087$ ) and 11.6 for the elliptic cone ( $\mu = 0.1$ ). The end of the cone at its largest diameter necessarily implies a more or less pronounced rounding and therefore a decreasing angle with easier penetration. A combination of these factors could explain the difference between theoretical and optimized values of A.

Considering the modelling leading to the definition of A and  $K_{fish}$ , these terms only depend on the fish and not on the mesh. We can hypothesize that, for a given fish, a larger mesh would allow a larger escape zone (e.g. grey area of Fig. 10, left), delimited by the fish isoline  $A \cdot F_p$ . However, experiments with different mesh sizes and twine diameters would be needed to test this hypothesis. The twine pressure on the fish skin depends on its diameter, which may affect the body depression d and the value of  $K_{fish}$ . A different mesh size could possibly modify the contact position with the fish and consequently its angle and friction coefficient involved in A.

The fish coefficient A was expected to be larger for fish than for rigid bodies (the fish friction and angle are supposedly lower than for plastic cones). However, the fish body becomes locally hollow under the twine pressure, which increases its angle locally. Thus, the effect of the fish angle on the value of A, when it comes to the largest and softer part of the body, is probably of lesser importance.

K1 and K2 seem to be independent of the perimeter range (or size range) for the same species as they fit the experimental data (Table 10). This needs confirmation for larger size ranges, especially for haddock, as the studied examples have a fairly narrow size range and with fish sizes close to the minimum commercial size. The mesh size was chosen so as to enable the model to explore a wider range of forces (FN, FT) and opening angles (more contact nodes, more opening variations) than for a larger mesh. As stated by Sistiaga et al. (2011), the fish used for fall-through experiments should not be affected by dehydration, depressurization or rigor mortis. We have not respected these conditions, although our objective was not to provide selectivity results. The choices made are coherent with the main objective of this study, to develop and validate a model to explore the mechanical interaction between mesh and fish. However, the model now requires validation on larger commercial meshes. Despite the choice of a simple linear elasticity model of the fish body, fish stiffness is difficult to interpret. The calculated dorsal and ventral stiffness did not differ as much as we would have expected (21% for haddock and 47% for horse mackerel), while horse mackerel stiffness was expected to be higher than haddock stiffness. In further work, these stiffnesses should be evaluated separately and not through an overall optimisation process.

The elliptical shape was chosen to model the fish cross-section to simplify its definition using a simple calliper and a measuring tape. It is simpler than the shapes used by Tokaç et al., 2016 ('superdrope',

'flexdrope', 'flexellipse' section models), but it enables good model agreement with experimental results. This can be explained by the coupled deformations of the mesh and of the fish, which leads to a kind of reciprocal self-adaptation and thus minimises the effect of the initial choice of cross-section shape. This can be illustrated for gillnet low mesh tension where the shape of the mesh adapts to the fish cross-section, regardless of its shape.

A strong and common hypothesis was made regarding propulsion force, which was supposed to be equal to the fish weight. However, if we consider the escape threshold fields (Fig. 10), we observe that the escape isolines are rather tight. Consequently, a variation in  $F_p$  in the threshold  $A \cdot F_p$  will lead to limited variation in  $(F_N, F_T)$  defining the mesh load that enables escape. Thus, based on these figures, we can conclude that fish propulsion force is not very sensitive to the escape threshold and that fish weight is a good proxy. Nevertheless, this modelling makes it possible to test other propulsion values.

Several sets of parameters per species are provided depending on the optimisation strategy: one per perimeter class, determined by optimizing each perimeter class in order to validate the model's results, and a second obtained by combining and optimizing all the perimeter classes of a species. For both species, the two strategies provide close escape threshold values and qualitatively discriminate the perimeter class, with classes differences between strategies remaining lower than the differences between classes. This means the proposed model is able to discriminate fish perimeter characteristics in the escape process. The latter strategy enables to extrapolate escape thresholds for missing perimeter classes which should, however, be confirmed with additional fall-through experiments on extreme size classes.

### **From a single mesh to netting**

The choice of the netting size (12 x 12 mesh) seems valid to evaluate the escape threshold but remains too small to consider the diameter ratio (for examples of differences between position and force conditions, see Fig. 16). For this purpose, more meshes would be needed. However, in a practical application, the boundary condition would be a mixed condition between force and position, imposed by neighbouring meshes, and the results would probably be intermediate between the force and position results shown in Fig. 16. Moreover, diameter ratio is not a key parameter but just a comparison with rigid frame fall-through experiments. A netting made of a stiffer material would probably need more meshes to avoid dependency on boundary conditions.

In T0 mode, the results obtained on a single mesh and on the 12 x 12 netting are very similar (escape threshold slopes in Table 11 compared with those of Table 9). Consequently, the threshold in the T0 mode obtained from a single mesh bench test could be directly applicable to a full-size netting.

In T90 mode, however, the escape threshold is modified: escape is easier compared with the single mesh results. Thus, additional simulations on netting will be needed once the fish coefficients are obtained from the bench test. The differences observed among case studies in terms of escape shift from a single T90 mesh to T90 netting could be explained by the fish section ellipticity and by the ratio of the fish perimeter to the mesh perimeter, particularly for low mesh tension. Effects of fish ellipticity and perimeter ratio should be analysed in further studies.

### **Comparison of escapes through a deformable mesh and a non-deformable mesh**

Our results show that a deformable mesh let larger fish escape than a rigid mesh in the load range and fish sample considered. This result is particularly sensitive in T90 mode for roundfish, highlighting the need to consider this deformability in selectivity studies involving fall through experimented.

The ability of T90 mesh to let bigger fish escape compared to a T0 mesh can be explained by the S bar shape of T90 (Fig. 12) that provides a 'deformability reserve' when the bars get tightened. In this case the mesh is distorted by the fish, so we should also question fish behaviour: would a fish try to escape through a mesh that is not perceived as being sufficiently open? Underwater recordings in trawls (Robert et al., 2020, pers. obs.), showing fish swimming a few moments inside the mesh before they succeed or not escaping suggests a positive answer to this question. However, fish have also been observed swimming close to open meshes and not trying to escape through them (Robert et al., 2020; Glass et al., 1993). More generally, fish behaviour is a major component in an escape attempt and also needs input. The dynamics of active swimming can also be more efficient for escape than the inert fish considered in this study.

The modelling developed and validated in this study, taking into account the hypothesis and the small number of fish tested, suggests that the success of escape attempts is underestimated on the basis of fall-through experiments in rigid mesh frames compared with a single deformable mesh. Additionally, applying the present results to netting would further increase escape success estimates with T90 mesh.

Future work should now consist in looking for a parameterized definition of the threshold map according to the size of the fish, which would then facilitate application of such an approach to a predictive selectivity model.

## **Conclusions**

An original model was developed and validated for a limited number of cases to study the escape mechanics of fish through a deformable mesh with different mechanical loads.

The results confirm an easier escape, i.e. with lower propulsion force or larger fish diameter, in T90 mode than in T0 mode for the same mesh load. For the studied cases, escape is even easier in T90 when considering a netting instead of a single mesh, particularly when the section of the fish is close to a circle and when the perimeter ratio (fish/mesh) is close to 1.

The deformation of the fish body under twine pressure requires further experimental exploration.

Mesh deformation due to a fish escape attempt allows fish of larger diameter to escape compared with rigid frame tests.

## **Acknowledgments**

This study was supported by France Filière Pêche and IFREMER (Institut Français de Recherche pour l'Exploitation de la Mer) from the 'Fusion-Scotch' support project. We deeply thank the anonymous reviewers for their comments and suggestions, which greatly improved the manuscript.

## References

- Coulomb, C.A., 1821. *Théorie des Machines Simples* 12.
- Cuende, E., Arregi, L., Herrmann, B., Sistiaga, M., Aboitiz, X., 2020. Prediction of square mesh panel and codend size selectivity of blue whiting based on fish morphology. *ICES J. Mar. Sci.* <https://doi.org/10.1093/icesjms/fsaa156>
- Digre, H., Hansen, U.J., Erikson, U., 2010. Effect of trawling with traditional and “T90” trawl codends on fish size and on different quality parameters of cod *Gadus morhua* and haddock *Melanogrammus aeglefinus*. *Fish. Sci.* 76, 549–559. <https://doi.org/10.1007/s12562-010-0254-2>
- Efanov, S.F., 1987. Influence of the form of fish body and mesh on selective properties of trawls. *J. Chem. Inf. Model.* 53, 1689–1699.
- Gatti, P., Méhault, S., Morandeau, F., Morfin, M., Robert, M., 2020. Reducing discards of demersal species using a 100 mm square mesh cylinder: Size selectivity and catch comparison analysis. *Mar. Policy* 116. <https://doi.org/10.1016/j.marpol.2019.103777>
- Glass, C.W., Wardle, C.S., 1995. Studies on the use of visual stimuli to control fish escape from codends. II. The effect of a black tunnel on the reaction behaviour of fish in otter trawl codends. *Fish. Res.* 23, 165–174. [https://doi.org/10.1016/0165-7836\(94\)00331-P](https://doi.org/10.1016/0165-7836(94)00331-P)
- Glass, C.W., Wardle, C.S., Gosden, S.J., 1993. Behavioural studies of the principles underlying mesh penetration by fish. *ICES Mar. Sci. Symp.* 196, 92–97.
- Herrmann, B., Krag, L.A., Frandsen, R.P., Madsen, N., Lundgren, B., Stæhr, K.J., 2009. Prediction of selectivity from morphological conditions: Methodology and a case study on cod (*Gadus morhua*). *Fish. Res.* 97, 59–71. <https://doi.org/10.1016/j.fishres.2009.01.002>
- Jones, E.G., Summerbell, K., O’Neill, F., 2008. The influence of towing speed and fish density on the behaviour of haddock in a trawl cod-end. *Fish. Res.* 94, 166–174. <https://doi.org/10.1016/j.fishres.2008.06.010>
- Kim, Y., 2019. Analysis on the body size selectivity for multi-species of discarding juvenile fishes in the bottom trawl. *J. Korean Soc. Fish. Technol.* 55, 181–189. <https://doi.org/10.3796/ksfot.2019.55.3.181>
- Krag, L.A., Herrmann, B., Madsen, N., Frandsen, R.P., 2011. Size selection of haddock (*Melanogrammus aeglefinus*) in square mesh codends: A study based on assessment of decisive morphology for mesh penetration. *Fish. Res.* 110, 225–235. <https://doi.org/10.1016/j.fishres.2011.03.009>
- Le Bris, F., Marichal, D., 1999. Numerical and experimental study of submerged flexible nets: Applications to fish farms. *Proc. 1999 Ninth Int. Offshore Polar Eng. Conf. (Volume 3)*, Brest, Fr. 30 May - 4 June 1999 749–755. <https://doi.org/10.1007/BF02492931>
- Luersen, M.A., Riche, R. Le, Guyon, F., 1884. A constrained , globalized , and bounded Nelder – Mead method for engineering optimization. <https://doi.org/10.1007/s00158-003-0320-9>
- Marais, J.F.K., 1985. Some factors influencing the size of fishes caught in gillnets in eastern cape estuaries. *Fish. Res.* 3, 251–261. [https://doi.org/10.1016/0165-7836\(85\)90026-8](https://doi.org/10.1016/0165-7836(85)90026-8)
- Mouchet, M., Poirson, M., Morandeau, F., Vogel, C., Méhault, S., Kopp, D., 2019. Using a trait-based

- approach to understand the efficiency of a selective device in a multispecific fishery. *Sci. Rep.* 9, 1–8. <https://doi.org/10.1038/s41598-019-47117-4>
- O’Neill, F.G., McKay, S.J., Ward, J.N., Strickland, A., Kynoch, R.J., Zuur, A.F., 2003. An investigation of the relationship between sea state induced vessel motion and cod-end selection. *Fish. Res.* 60, 107–130. [https://doi.org/10.1016/S0165-7836\(02\)00056-5](https://doi.org/10.1016/S0165-7836(02)00056-5)
- O’Neill, F.G., Summerbell, K., 2019. The influence of continuous lines of light on the height at which fish enter demersal trawls. *Fish. Res.* 215, 131–142. <https://doi.org/10.1016/j.fishres.2019.03.010>
- Priour, D., De La Prada, A., 2015. An experimental/numerical study of the catch weight influence on trawl behavior. *Ocean Eng.* 94, 94–102. <https://doi.org/10.1016/j.oceaneng.2014.11.016>
- Purbayanto, A., Monintja, D.R., Tsunoda, A., Arimoto, T., 2003. Selectivity , Survival , and Stress of Japanese Whiting *Sillago japonica* after Simulated Capture by a Sweeping Trammel Net. *Am. Fish. Soc. Symp.* 1–11.
- Regulation (EU), 2013. REGULATION (EU) No 1380/2013 OF THE EUROPEAN PARLIAMENT AND OF THE COUNCIL of 11 December 2013 on the Common Fisheries Policy, amending Council Regulations (EC) No 1954/2003 and (EC) No 1224/2009 and repealing Council Regulations (EC) No 2371/2002 and (EC. <https://doi.org/https://eur-lex.europa.eu/eli/reg/2013/1380/oj>
- Reis, E.G., Pawson, M.G., 1999. Fish morphology and estimating selectivity by gillnets. *Fish. Res.* 39, 263–273. [https://doi.org/10.1016/S0165-7836\(98\)00199-4](https://doi.org/10.1016/S0165-7836(98)00199-4)
- Robert, M., Cortay, A., Morfin, M., Simon, J., Morandeau, F., Deneubourg, J.L., Vincent, B., 2020. A methodological framework for characterizing fish swimming and escapement behaviors in trawls. *PLoS One* 15, 1–17. <https://doi.org/10.1371/journal.pone.0243311>
- Tokaç, A., Herrmann, B., Gökçe, G., Krag, L.A., Nezhad, D.S., 2018. The influence of mesh size and shape on the size selection of european hake (*Merluccius merluccius*) in demersal trawl codends: An investigation based on fish morphology and simulation of mesh geometry. *Sci. Mar.* 82, 147–157. <https://doi.org/10.3989/scimar.04764.18A>
- Tokaç, A., Herrmann, B., Gökçe, G., Krag, L.A., Nezhad, D.S., Lök, A., Kaykaç, H., Aydın, C., Ulaş, A., 2016. Understanding the size selectivity of red mullet (*Mullus barbatus*) in Mediterranean trawl codends: A study based on fish morphology. *Fish. Res.* 174, 81–93. <https://doi.org/10.1016/j.fishres.2015.09.002>
- Villarino, M., 2006. A note on the accuracy of Ramanujan’s approximative formula for the perimeter of an ellipse. *J. Inequalities Pure Appl. Math.* 7, 1–10.
- Vincent, B., Simon, J., Cesare, N. Di, 2020. Development of a model for flexural rigidity of fishing net with a spring mass approach and its inverse identification by metaheuristic parametric optimization. *Ocean Eng.* 203, 107166. <https://doi.org/10.1016/j.oceaneng.2020.107166>
- Yamaguchi Y., 1994. Frottement des plastiques. *Techniques de l’Ingénieur.*
- Sistiaga, M., Herrmann, B., Nielsen, K.N., Larsen, R.B., 2011. Understanding limits to cod and haddock separation using size selectivity in a multispecies trawl fishery: An application of FISHSELECT. *Can. J. Fish. Aquat. Sci.* 68, 927–940. <https://doi.org/10.1139/f2011-017>